ELSEVIER

Computers in Biology and Medicine 36 (2006) 209–223

Computers in Biology and Medicine

www.intl.elsevierhealth.com/journals/cobm

Optical imaging of breast tumor through temporal log-slope difference mappings

Zhixiong Guo[a,*], Siew Kan Wan[a], David A. August[b,c], Jinpin Ying[d], Stanley M. Dunn[e], John L. Semmlow[c,e]

[a] *Department of Mechanical and Aerospace Engineering, Rutgers, The State University of New Jersey, 98 Brett Road, Piscataway, NJ 08854, USA*

[b] *The Cancer Institute of New Jersey, University of Medicine and Dentistry of New Jersey, New Brunswick, NJ 08903, USA*

[c] *Department of Surgery, UMDNJ Robert Wood Johnson Medical School, New Brunswick, NJ 08901, USA*

[d] *Bell Labs, Lucent Technologies, Holmdel, NJ 07733, USA*

[e] *Department of Biomedical Engineering, Rutgers, The State University of New Jersey, Piscataway, NJ 08854, USA*

Received 6 November 2003; accepted 30 September 2004

Abstract

A novel optical temporal log-slope difference mapping approach is proposed for cancerous breast tumor detection. In this method, target tissues are illuminated by near-infrared (700–1000 nm) ultrashort laser pulses from various surface source points, and backscattered time-resolved light signals are collected at the same surface points. By analyzing the log-slopes of decaying signals over all points on the source-detection grid, a log-slope distribution on the surface is obtained. After administration of absorption contrast agents, the presence of cancerous tumors increases the decaying steepness of the transient signals. The mapping of log-slope difference between native tissue and absorption-enhanced cancerous tissue indicates the location and projection of tumors on the detection surface. In this paper, we examine this method in the detection of breast tumors in two model tissue phantoms through computer simulation. The first model has a spherical tumor of 6 mm in diameter embedded at the tissue center. The second model is a large tissue phantom embedded with a non-centered spherical tumor 8 mm in diameter. Monte Carlo methods were employed to simulate the light transport and signal measurement. It is shown that the tumor in both the tissue models will be accurately projected on the detection surface by the proposed log-slope

* Corresponding author. Tel.: +1 732 445 2024; fax: +1 732 445 3124.
E-mail address: guo@jove.rutgers.edu (Z. Guo).

0010-4825/$ - see front matter
doi:10.1016/j.compbiomed.2004.09.003

difference mapping method. The image processing is very fast and does not require any inverse optimization in image reconstruction.

Keywords: Near-infrared imaging; Breast cancer detection; Temporal log-slope; Absorption contrast agent; Ultrafast laser; Monte Carlo method; Simulation

1. Introduction

Cancer is the second leading cause of death among Americans. The American Cancer Society estimated that, in 2002, about 1.3 million Americans received new diagnosis of cancer and about 550 thousand died from this disease [1]. Early diagnosis is thought to represent an important opportunity to reduce both the morbidity and mortality that result from cancer. X-rays are commonly utilized for cancer screening and diagnosis. Chest X-rays, computed tomography, and mammography are the most commonly used modalities, but these methods can be costly and induce radiation exposure. Therefore, a great need exists for new non-invasive methods that pose less safety concerns, are low cost, portable and can be made widely available to large segments of the population.

Optical imaging methods are excellent candidates to provide an alternative imaging modality. Near-infrared (NIR) optical imaging has become increasingly attractive in recent years because NIR radiation is non-ionizing and the approach can lead to devices that are very compact and cost-effective. Furthermore, optical imaging can provide not only structural information [2–9] and functional information [10–13], but also cellular and molecular information [14,15].

Wavelengths in the NIR range, especially between 700 and 1000 nm are widely used in research for diffuse optical tomography (DOT) because this spectral window has the lowest overall tissue absorption. In other words, light in that range has a much greater penetration depth allowing deep imaging up to several centimeters. This is sufficient for many potential clinical applications, such as breast cancer screening and diagnosis. In DOT techniques, the target tissue is illuminated by a NIR laser (either pulsed or continuous-wave). Measurements of light signals (in either time- or frequency-domain) around the tissue boundary are made and used to reconstruct tissue images of optical parameters. Diseases are detected and/or diagnosed based on the difference of optical properties between normal and diseased tissues.

The most challenging task in utilizing DOT is the fact that NIR light is highly scattered in human tissues. Unlike X-ray and PET that depend on the ballistic transmitted component of radiation emission, optical imaging has to deal with highly diffused and back-scattered light during image reconstruction. For highly diffused NIR light in biologic tissues, the temporal and/or spatial intensity response sensed by a detector is not only determined by the optical properties along a direct path between the source and detector, but also by the optical properties in large surrounding regions as described in random walk theory. Therefore, the image reconstruction in DOT is a formidable inverse problem, in which the tissue optical properties from a given experimental setup and a given set of measurements are determined through an optimization process using predicted boundary measurements in forward modeling with pre-assumed optical tissue parameters. An inverse process may easily require dozens of and hundreds of times of forward modeling. Previously most forward modeling approaches use a simplified diffusion approximation [16]. Rigorous radiation transfer simulation [17,18] is more appropriate, however, because biologic tissues are generally heterogeneous and may contain low-scattering and/or high-absorbing

regions. Given the complexity of both the distribution of tissue optical properties and a forward model approach, an image reconstruction in a typical DOT may take several hours to several days even with the latest computation technology. Further, an inverse problem in DOT is usually ill-posed and may lead to divergent results.

A much faster method to detect tumors can be based on the relative absorption contrast between the cancerous tumors and surrounding normal tissues, rather than the solution of the distributions of tissue optical parameters. Some recent reports have shown that the NIR absorption in cancerous regions can be greatly enhanced by the addition of absorbing dyes that have close affinity to the tumor. For example, indocyanine green dyes were used by Ntziachristos et al. [13] and Roy et al. [4]. The strong absorption will have a greater attenuation effect on the light signals detected at the tissue surface, especially for detectors most closely located to the cancerous tumor. This will result in an increase of decaying steepness in the temporal light signals. By measuring the temporal slopes of the logarithmically decaying signals over all detection points, a log-slope distribution on the tissue surface is obtained. The area with large log-slope values may represent a projection of tumors. In this approach, the complicated inverse image reconstruction is avoided.

The feasibility of log-slope approach in detecting a highly absorbing inhomogeneity in turbid media has been recently demonstrated [19] both experimentally and through simulation using a tiny graphite inclusion inside a homogeneous tissue phantom. This method is designed to accommodate the requirements of an inexpensive and rapid screening tool to detect the presence of tumors in human body before performing a comprehensive tomographic scan or biopsy examination. It was motivated by several published studies [17,18,20–25] that investigated the laser pulse response of both transmitted and backscattered signals in turbid media. Brewster and Yamada [21] found that the asymptotic log-slope of a simulated signal in a homogeneous semi-infinite slab increases as the scattering albedo decreases and vice versa. Zaccanti et al. [22] showed a significant dependence between the scattering coefficient of a homogeneous medium and the broadening of a laser pulse: this broadening also affected the steepness of the pulse's decaying slope. Recent studies by Guo and his coauthors [17,18] extended these transient laser pulse investigations to two- and three-dimensional inhomogeneous tissue phantoms. They observed variations in the temporal log-slope of the detected signals in the presence of a relatively high absorbing tumor in the tissue phantoms.

In the direct log-slope approach, however, there is a fuzzy boundary around the absorbing inhomogeneous area and the edge effect [19] (signals decay fast in detectors located near surface edge) on the detecting surface is very pronounced. Here we propose a modified version of log-slope approach, i.e., mapping of temporal log-slope difference on the detection surface between log-slope distributions before and after administration of absorption contrast agent. Such a subtraction operation will eliminate the edge effect and diminish the fuzzy boundary of images.

In this paper, the feasibility of the temporal log-slope difference mapping approach for cancer detection is studied by simulating light propagation in two tissue phantoms implanted with spherical tumors and evaluating the light detected from a coincident laser source over a predefined grid on the tissue surface. The propagation of photons in the tissue phantoms is simulated via our 3-D transient Monte Carlo radiative transfer method [23,24]. We present a comprehensive description to the simulation models as well as the modified Monte Carlo treatment of light transport in tissues with the presence of tumor. This is followed by a discussion of the analysis techniques applied to the detected signals to construct 2-D log-slope difference mappings that lead to the detection of cancerous tumor. Following this discussion, the detected 2-D images of simulated tumors in the two tissue models will be presented.

2. Modeling and imaging

This study investigates two simulation models. The first model consists of a homogeneous cuboidal tissue phantom embedded with a spherical tumor located at the center (Fig. 1a). The tissue phantom's dimensions are $20\times20\times20\,\text{mm}^3$, and the spherical tumor has a diameter of 6 mm. The NIR optical properties of the tissue phantom have been assigned to mimic biologic tissue. We assume the reduced scattering and absorption coefficients of the tissue are 1.0 and $0.005\,\text{mm}^{-1}$, respectively. These typical values are selected in line with the studies in the literature [2–11]. Optical properties of living tissue vary with light wavelength and physiological functions. The measured optical properties for different individuals are also different. All these will tremendously complicate the clinical use of conventional DOT techniques. However, they do not practically influence the present imaging method because the present method is based on the detection of relative absorption change. The exact value of tissue optical properties and their variations in actual tissues are insignificant. Hence, we may assume a homogeneous profile for tissue optical properties when contrast agents are used. The difficulty in the treatment of the heterogeneity of tissue structure and properties is overcome in this imaging method.

After injection of absorbing dyes, the absorption coefficient in the cancerous tumor region is assumed to be $0.2\,\text{mm}^{-1}$, while it is $0.01\,\text{mm}^{-1}$ in the healthy tissue region. This corresponds to an absorbing dye uptake ratio of 39:1. The absorption contrast between the absorption-enhanced tumor and the healthy tissue is therefore 20:1. The absorption coefficient of malignant cancerous tissue is greater than that of healthy tissue, because increased blood flow leads to higher concentration or accumulation of oxy- and deoxy-hemoglobin (two natural absorbing chromophores inside human body at NIR wavelengths). As compared with the significant absorption augmentation through absorbing dye administration, however, this natural absorption contrast between cancerous and healthy tissues is negligible.

The second simulation model features a larger tissue phantom with an off-centered tumor (Fig. 1b). The dimensions of the tissue phantom increase to $40\times40\times30\,\text{mm}^3$ and the diameter of the tumor is 8 mm. The tumor center is located at the position of ($x = 24$ mm, $y = 24$ mm, and $z = 15$ mm). All the optical properties except for the contrast-enhanced absorption coefficient in the tumor remain the

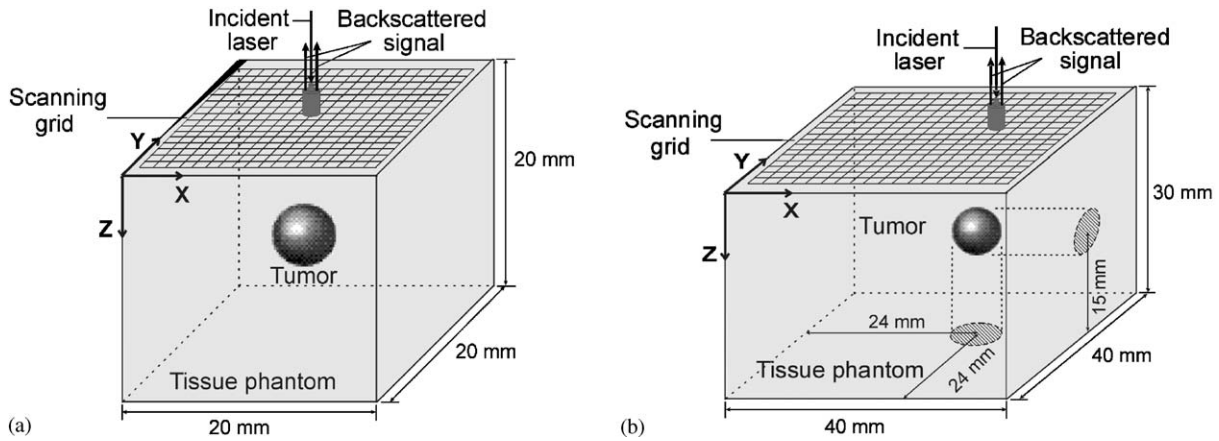

Fig. 1. (a) Detection model I: a spherical tumor of 6 mm in diameter embedded at the center of a $20\times20\times20\,\text{mm}^3$ tissue phantom; and (b) detection model II: a spherical tumor of 8 mm in diameter embedded inside a $40\times40\times30\,\text{mm}^3$ tissue phantom.

same as those assumed in the first simulation model. The absorption coefficient of the cancerous tumor is changed to $0.25\,\mathrm{mm}^{-1}$, increasing the absorption contrast between the tumor and the healthy tissue to 25:1. This model is chosen to test the ability of the log-slope difference mapping approach to detect and locate a tumor when the edge effect [19] in the determination of log-slopes is appreciable. The refractive index for both the tissue phantoms and tumors in the models are assumed to be $n = 1.4$.

The laser delivery and detection system is set up so that the incident laser and backscattered signal coincide with each other. Ultrafast laser pulses are set to be delivered across a circular area with an effective radius of 0.1 mm. The intensity distribution is assumed to be a Gaussian profile with its peak intensity located at the center of the circular area. The scanning grid for detection model I consists of a 19×19 equally spaced mesh with a resolution of 1mm. Due to the symmetry of this detection model, only one-fourth of the scanning grid results are needed in simulation. For detection model II with an off-centered tumor, the calculations are performed over an 11×11 scanning grid with a resolution of 2 mm. The scanning grids span from $x = 14$ to 34 mm and $y = 14$ to 34 mm, respectively. In practical use, of course, the scanning grid must cover the whole surface because presence of a tumor or tumors and their location(s) are unknown.

The simulation of experimental set-up including light illumination and signal measurements is executed using a Monte Carlo program adapted from Guo et al. [24]. Modifications have been made to the program code to consider the presence of tumors. The Monte Carlo simulation mimics photon propagation by calculating the random walks of a large number of photon bundles. Each emitted photon bundle begins from its initial position and time before making its way into the participating medium by a certain path length determined from statistical distribution and given by the equation:

$$l = -\frac{1}{\mu_\mathrm{e}}\ln(\Re), \tag{1}$$

where μ_e represents the extinction coefficient of the medium and $\Re$ the random number generated by the computer. The photon bundle will experience scattering, absorption, or reflection at tissue–air interfaces before being detected. Fresnel reflection [18] at the tissue–air boundary is considered because there is a significant refractive index mismatch between tissue and air. Total internal reflection occurs when the incoming angle is not less than the critical angle as determined by Snell's law. The energy attenuation due to absorption is calculated using the Beer–Lambert law:

$$I_{i+1} = I_i \mathrm{e}^{-\mu_\mathrm{a} l}, \tag{2}$$

where I_i and I_{i+1} are photon bundle energy before and after each scattering event, respectively, l is the path length calculated from Eq. (1), and μ_a is the absorption coefficient of the medium along each scattering path length and varies depending on whether it is inside healthy tissue or inside the tumor. In the event where the photon bundle's path traverses both the normal tissue and tumor regions, the overall energy attenuation is calculated from two successive attenuations in the tissue and tumor regions, respectively. The first attenuation will be based on the distance to the tissue–tumor interface with the current extinction coefficient, while the second attenuation is based on the remaining path length with the extinction coefficient corresponding to the medium that the photon bundle is traveling towards. The remaining path length l_2 is calculated based on the conservation of optical depth and is given by:

$$l_2 = \frac{\mu_{\mathrm{e}1}(l_0 - l_1)}{\mu_{\mathrm{e}2}}, \tag{3}$$

where l_0 corresponds to the path length of the originally intended travel distance calculated from Eq. (1), and l_1 corresponds to the distance to the tissue–tumor interface from the starting point. The constants μ_{e1} and μ_{e2} refer to the extinction coefficients of the medium before and after the tissue–tumor interface. In our simulation, we used a total of 10^8 photon bundles on each node of the scanning grid.

A single detecting point calculation takes about 2 h on a DELL PC equipped with a 1.7 GHz Pentium 4 processor and 256 MB memory. The simulation on the top surface of the tissue phantom requires 361 runs for detection model I with a 19×19 scanning grid and 121 runs for detection model II with an 11×11 scanning grid, respectively. The calculation task is too heavy for a single PC. Accordingly, the final calculations were conducted in a 64-CPU workstation cluster.

It must be pointed out that the above-mentioned computational effort was for simulating an experimental setup to obtain a "simulated" measurement. It is not used for image processing and reconstruction. If a practical experiment is set up, real measurement can be completed in minutes, and the previous simulation process is not necessary.

Due to the high-scattering and low-absorption of NIR light in tissues, detected signal pulses at the boundary will be broadened considerably. At the decaying part of the signal, there exists an asymptotic log-slope region that is sensitive to the distribution of absorption coefficients inside the tissue phantom. From our experience, the log-slope is best chosen in the time range of 300–700 ps. Prior to 300 ps the logarithmic signal is non-linear, while after 700 ps the signal strength is weak and the signal is strongly affected by a large zone beyond the optical axis. Fig. 2 shows the temporal signal profile detected from one location in Model I and the determination of asymptotic log-slope. In a recent paper [19], we have discussed the measurement of time-resolved log-slopes in detail.

In order to form a 2-D mapping of log-slope difference to detect the tumor's projection onto the tissue surface, we first evaluate the log-slope distribution before the administration of absorbing contrast agent. This evaluation is followed by evaluation of the log-slope distribution after absorption enhancement.

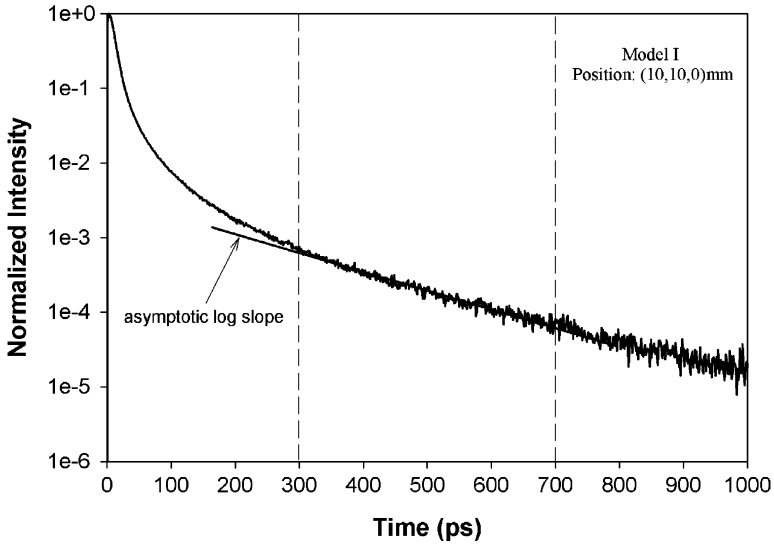

Fig. 2. A representative temporal signal profile and the determination of asymptotic log-slope.

Then, a 2-D mapping of log-slope difference between these two log-slope distributions can be constructed. Due to the affinity of absorbing contrast agent for cancerous regions, the log-slope difference is significantly larger in the tumor region than in other regions. This mechanism is illustrated in Fig. 3 which shows log-slope profiles versus x-position plotted along $y = 10$ mm for the first detection model in three different cases: before absorption enhancement, after absorption enhancement, and the net difference between the previous two profiles.

For each detection model, we obtained two sets of log-slope distributions corresponding to the cases before and after the addition of contrast agent, respectively. By proceeding with the log-slope subtraction process, a log-slope difference mapping was constructed. In the cancerous region, the difference is large. A final filtering process was applied to highlight the image contrast and to suppress unwanted noise. Values below a pre-assigned cut-off filter level were removed. The computation in

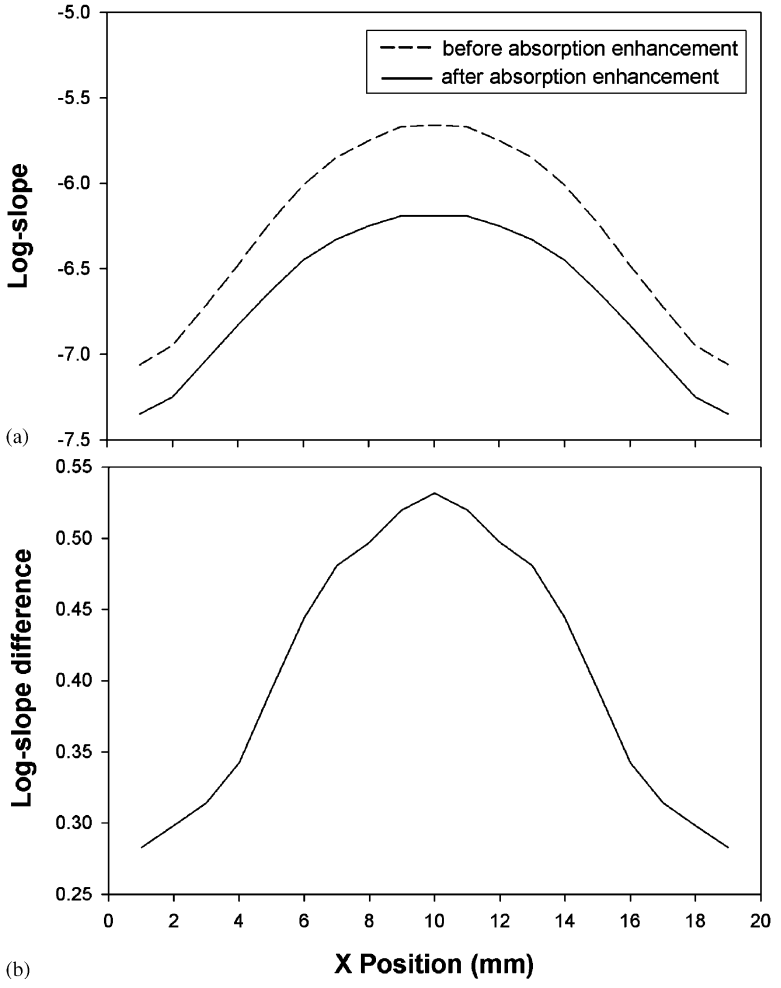

Fig. 3. (a) Plots of log-slope versus x-position along $y = 10$ mm for detection model I; and (b) profile of log-slope difference.

image processing and mapping construction took between 2 and 3 min on a DELL PC with one 1.7 GHz Pentium 4 CPU.

3. Results and discussion

The complete log-slope distributions of detection model I are presented in Figs. 4a and b. Fig. 4a shows the log-slope mapping on a surface of the cuboidal tissue phantom before administration of absorbing contrast agent. The log-slope values range from −5.60 to −8.80. The presence of tumor is not immediately identifiable due to the strong edge effect associated with the relatively small geometry in this detection model. Fig. 4b shows the result after absorption enhancement. The log-slope values range from −6.20 to −9.20. The absolute values of the log-slopes increase. This indicates that the decay of the log-slope signal has become steeper since more energy is absorbed by the absorption-enhanced tumor.

Fig. 5 a was obtained by subtracting the log-slopes in Fig. 4b from the corresponding values in Fig. 4a. The initial subtraction created log-slope difference values that fell between 0.05 and 0.53 for the whole 2-D distribution. A larger difference value indicates stronger absorption augmentation in the cancerous region. In this simulation result, the majority of the higher values (above 0.42) were concentrated on the region where the tumor is located. The presence of tumor at the center in Fig. 5a is clearly visible. Figs. 5b–5d show images of the tumor projection on the detection surface after applying various filters to the image in Fig. 5a. The cut-off filter value is 60% of the peak log-slope difference value in Fig. 5b, 70% in Fig. 5c, and 80% in Fig. 5d, respectively. As the cut-off filter value increased, the effective imaging area representing the tumor projection decreased accordingly. A 70% cut-off filter level was found to produce images clear enough for visualizing the tumor projection (indicated by the white circle in the figures). A more general and effective cut-off filter value can be established when more cases are simulated and analyzed. Although the filtered log-slope difference image corresponds well to the shape and location of the actual tumor, the image boundary does not resemble a perfect circle. The main reason is due to the limited resolution of the scanning grid defined in the simulation model. Further increase in resolution should result in a better image quality.

The images for detection model II are displayed in Figs. 6 and 7. Images are displayed in only part of the top surface of the tissue in order to save computational time used for simulating experimental measurements (the Monte Carlo simulation is computationally intensive. It is not the time for image processing and reconstruction). The tumor projection in Fig. 7 looks as though it were located at the center of the partial surface, but it is not at the center of the entire top surface.

Fig. 6a portrays the 2-D distribution of log-slopes for the tissue before contrast agent administration. The log-slope values are between −5.59 and −6.74. The edge effect is obvious. The log-slope distribution after absorption enhancement is presented in Fig. 6b where the log-slope values range from −5.67 to −7.10. Unlike detection model I in which the absorption contrast was only 20:1, the presence of tumor in detection model II (Fig. 6b. Absorption contrast increased to 25:1) is immediately noticeable even before the subtraction of two log-slope distributions. However, the boundary is very fuzzy.

Fig. 7a shows the mapping of log-slope difference between the two log-slope profiles in Fig. 6. The tumor presence is detected around the partial surface center at ($x = 24$ mm, $y = 24$ mm). After filtration with a cut-off filter value of 70% of the peak value, the shape and location of the tumor are clearly seen in Fig. 7b. The white circle is used to compare the actual size and location of the spherical tumor projection. The oscillation of the detected tumor projection boundary is well confined within the limit of detection resolution.

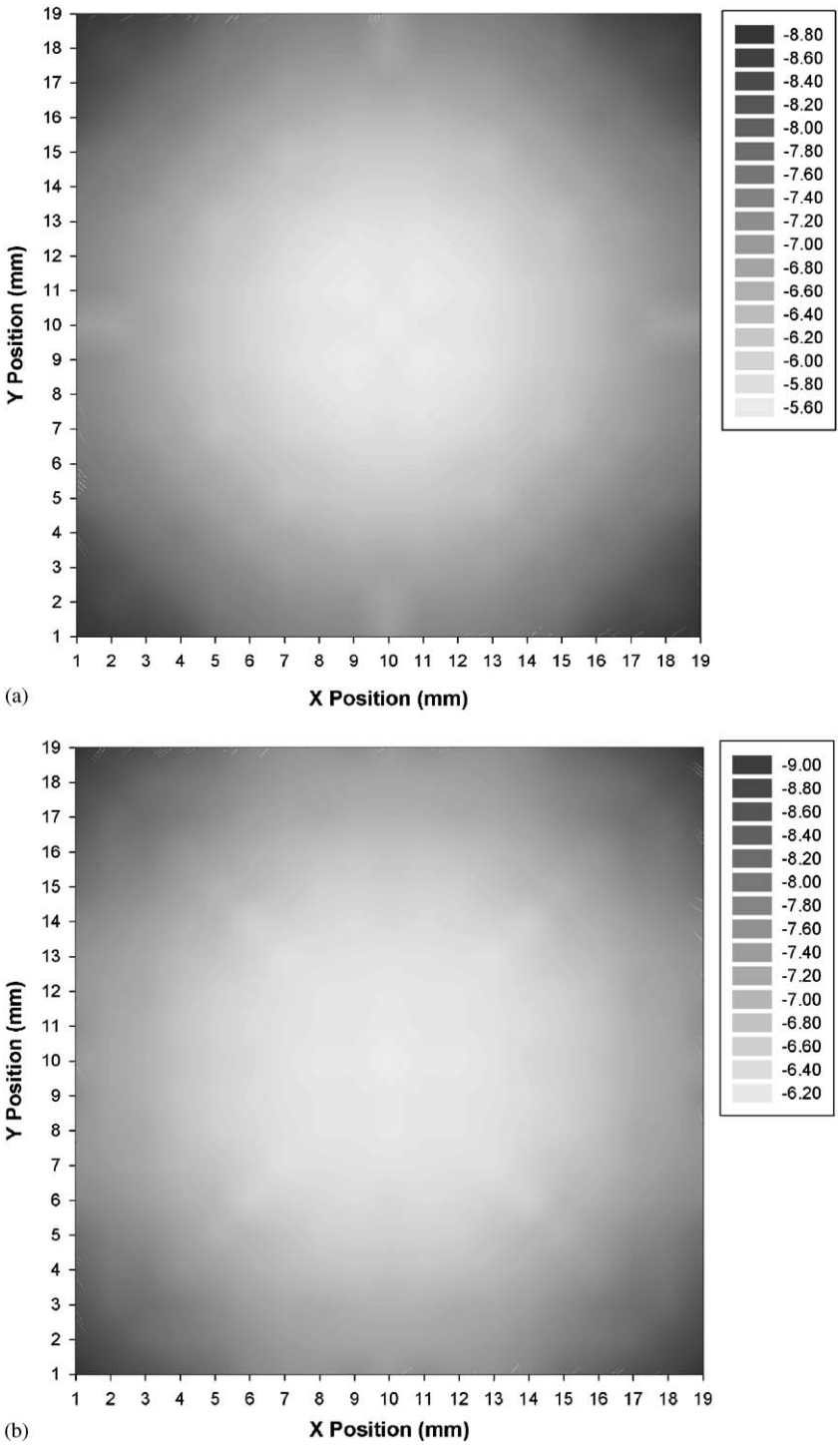

Fig. 4. Log-slope mapping results for detection model I: (a) before administration of contrast agent; and (b) after administration of absorption contrast agent.

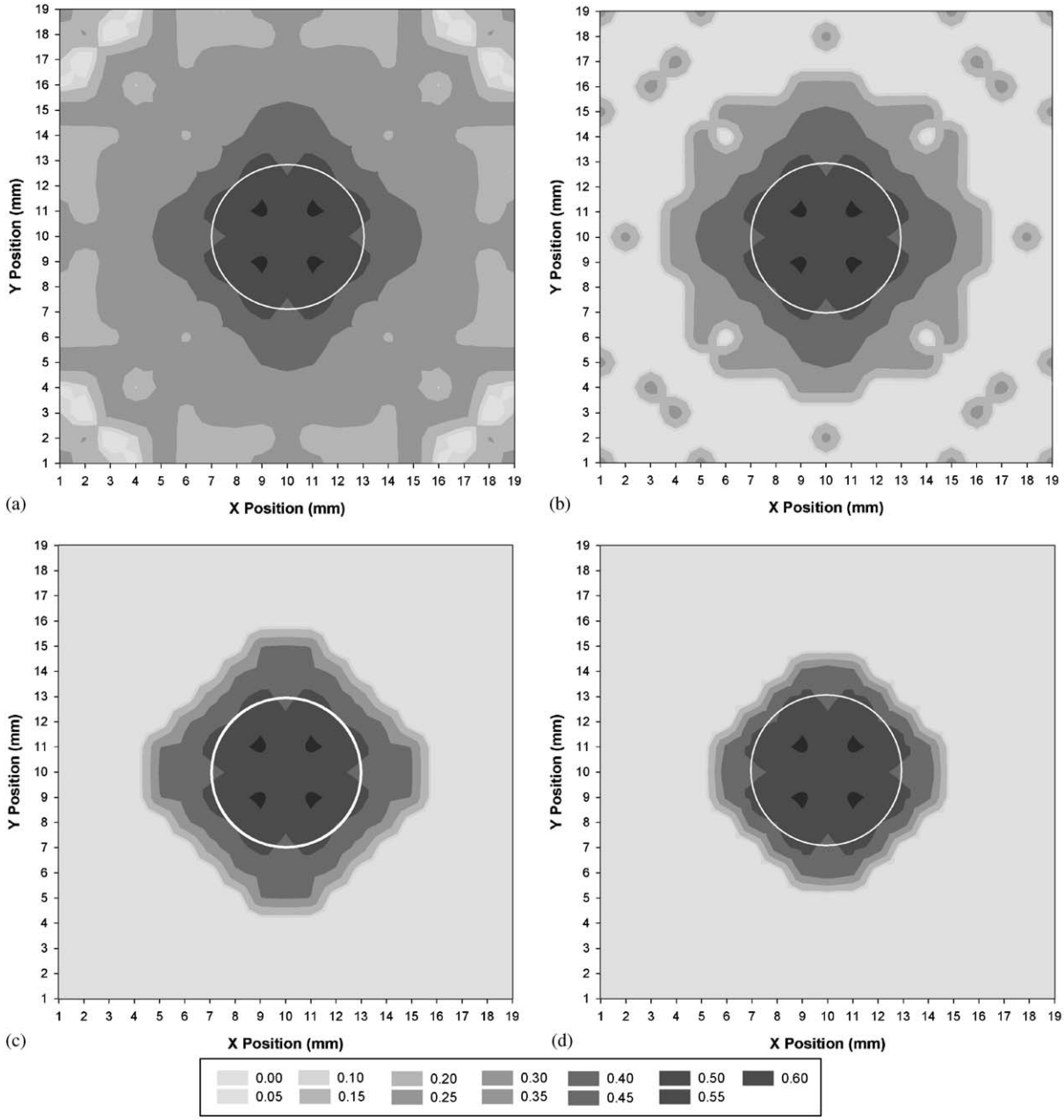

Fig. 5. Mappings of log-slope difference for detection model I: (a) initial result; (b) with 60% cut-off filter; (c) with 70% cut-off filter; and (d) with 80% cut-off filter.

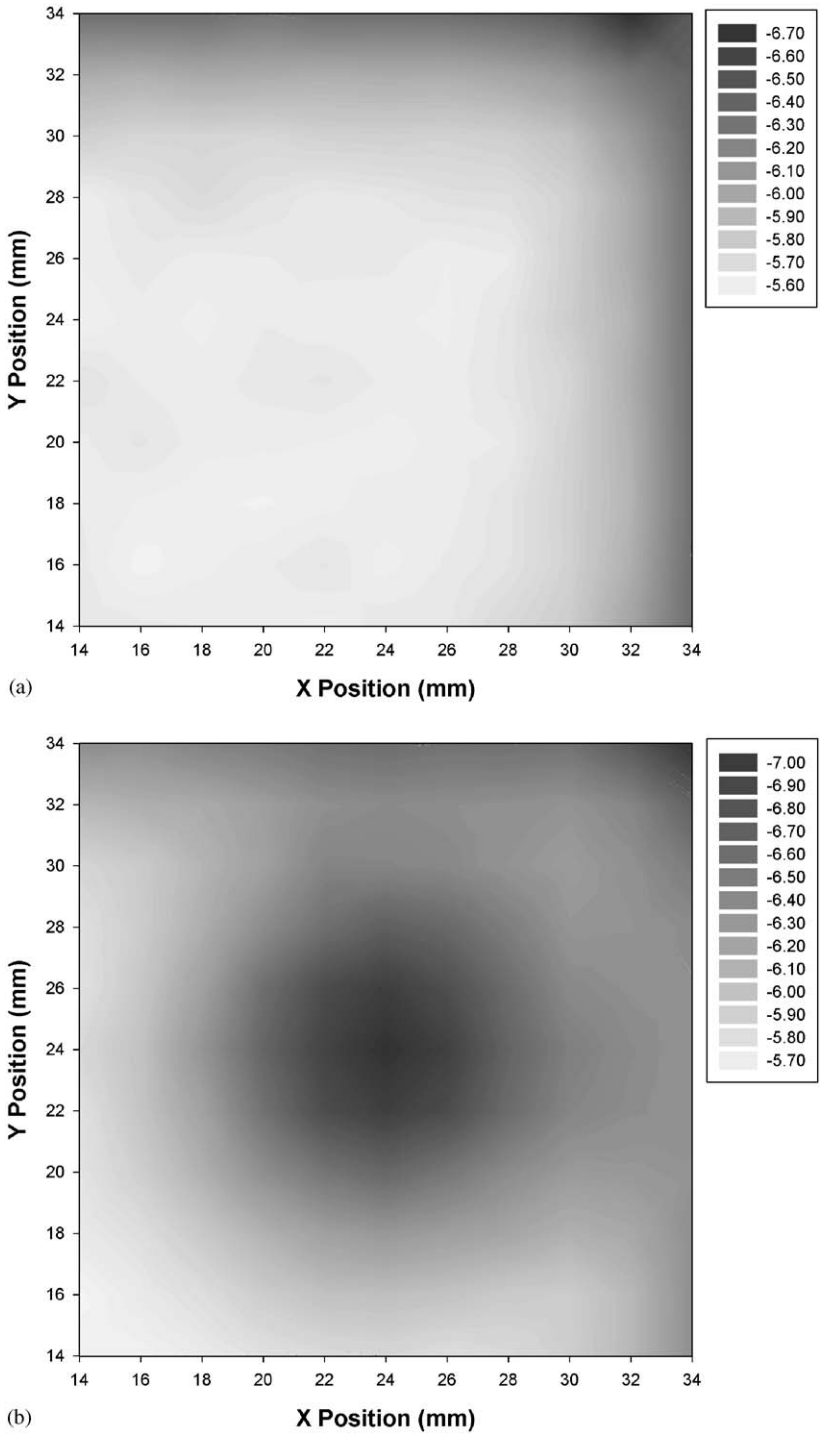

Fig. 6. Log-slope mapping results for detection model II: (a) before administration of contrast agent; and (b) after administration of contrast agent.

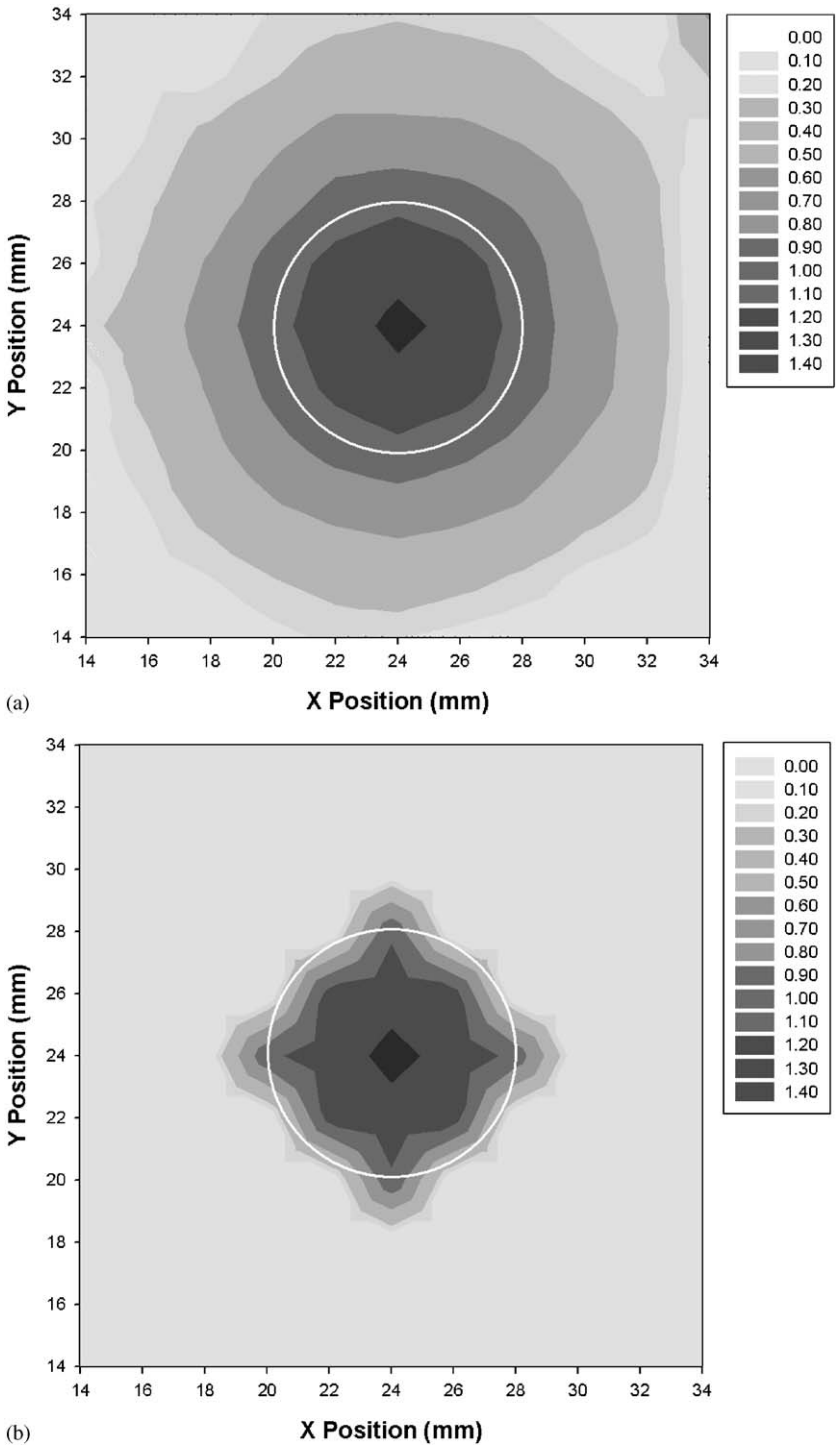

Fig. 7. Mappings of log-slope difference for detection model II: (a) initial result; and (b) with 70% cut-off filter.

4. Conclusions

This study evaluated a novel breast tumor detection method based on NIR log-slope difference mapping. The feasibility of this approach as a quick yet accurate preliminary diagnostic tool for early breast tumor detection was demonstrated numerically. The temporal log-slope difference between tissues before and after absorption enhancement was shown to be very large for those detection points directly above the embedded tumor. The results in the two example detection models accurately showed the shape and location of the embedded tumors. The proposed temporal log-slope difference mapping method is capable of forming 2-D tumor projection for the detection of cancerous tumors. The images were directly constructed. The image processing and construction took only 2–3 min in a PC. The present imaging method does not require any inverse image reconstruction. These features will greatly enhance the clinical utility of the present method.

We have shown this projection imaging capability for only one surface of the tissue. Clearly this method can produce log-slope difference mappings for multiple scanning surfaces throughout the entire tissue. The projection of the tumor onto multiple surfaces would produce log-slope difference maps that can be combined to produce a 3-D image. This as well as real experimental study will be the focus of our next report.

Acknowledgements

Z. Guo Acknowledges the partial support of this research from the New Jersey Space Grant Consortium, the Charles and Johanna Busch Memorial Fund, and the NSF Grant CTS-0318001.

References

[1] American Cancer Society, Cancer Facts & Figures, http://www.cancer.org/downloads/STT/CAFF2003PWSecured.pdf, 2003.
[2] B. Tromberg, A. Yodh, E. Sevick-Muraca, D. Pine, Diffusing photons in turbid media: introduction to the feature, Appl. Opt. 36 (1997) 9–231.
[3] M.J. Holboke, B.J. Tromberg, X. Li, N. Shah, J. Fishkin, D. Kidney, J. Butler, B. Chance, A.G. Yodh, Three-dimensional diffuse optical mammography with ultrasound localization in a human subject, J. Biomed. Opt. 5 (2000) 237–247.
[4] R. Roy, A. Godavarty, E.M. Sevick-Muraca, Fluorescence-enhanced optical tomography using referenced measurements of heterogeneous media, IEEE Trans. Med. Imag. 22 (2003) 824–836.
[5] J.C. Hebden, H. Veenstra, H. Dehghani, E.M.C. Hillman, M. Schweiger, S.R. Arridge, D.T. Delpy, Three-dimensional time-resolved optical tomography of a conical breast phantom, Appl. Opt. 40 (2001) 3278–3287.
[6] J.P. Culver, R. Choe, M.J. Holboke, L. Zubkov, T. Durduran, A. Slemp, V. Ntziachristos, B. Chance, A.G. Yodh, Three-dimensional diffuse optical tomography in the parallel plane transmission geometry: evaluation of a hybrid frequency domain/continuous wave clinical system for breast imaging, Med. Phys. 30 (2) (2003) 235–247.
[7] B.W. Pogue, S. Geimer, T.O. McBride, S.D. Jiang, U.L. Osterberg, K.D. Paulsen, Three-dimensional simulation of near-infrared diffusion in tissue: boundary condition and geometry analysis for finite-element image reconstruction, Appl. Opt. 40 (2001) 588–600.
[8] M.A. Bartlett, H. Jiang, Effect of refractive index on the measurement of optical properties in turbid media, Appl. Opt. 40 (10) (2001) 1735–1741.
[9] J. Wu, L. Perelman, R.R. Dasari, M.S. Feld, Fluorescence tomographic imaging in turbid media using early-arriving photons and Laplace transforms, PNAS 94 (1997) 8783–8788.

[10] D.A. Benaron, S.R. Hintz, A. Villringer, D. Boas, A. Kleinschmidt, J. Frahm, C. Hirth, H. Obrig, J.C. van Houten, E.L. Kermit, W.F. Cheong, D.K. Stevenson, Noninvasive functional imaging of human brain using light, J. Cereb. Blood Flow Metab. 20 (2000) 469–477.

[11] B.J. Tromberg, N. Shah, R. Lanning, A. Cerussi, J. Espinoza, T. Pham, L. Svaasand, J. Butler, Non-invasive in vivo characterization of breast tumor using photon migration spectroscopy, Neoplasia 2 (2000) 1–15.

[12] D.A. Boas, G. Strangman, J.P. Culver, R.D. Hoge, G. Jasdzewski, R.A. Poldrack, B.R. Rosen, J.B. Mandeville, Can the cerebral metabolic rate of oxygen be estimated with nearinfrared spectroscopy?, Phys. Med. Biol. 48 (2003) 2405–2418.

[13] V. Ntziachristos, A.G. Yodh, M. Schnall, B. Chance, Concurrent MRI and diffuse optical tomography of breast after indocyanine green enhancement, PNAS 97 (6) (2000) 2767–2772.

[14] E. Betzig, Proposed method for molecular optical imaging, Opt. Lett. 20 (3) (1995) 237–239.

[15] R. Weissleder, C.H. Tung, U. Mahmood, A. Bogdanov Jr., In vivo imaging of tumor with protease-activated near-infrared fluorescent probes, Nat. Biotech. 17 (1999) 375–378.

[16] Z. Guo, S.K. Wan, K.-H. Kim, C. Kosaruja, Comparing diffusion approximation with radiation transfer analysis for light transport in tissues, Opt. Rev. 10 (5) (2003) 415–421.

[17] Z. Guo, Kumar, Discrete ordinates solution of short pulse laser transport in two-dimensional turbid media, Appl. Opt. 40(19) (2001) 3156–3163.

[18] Z. Guo, K.H. Kim, Ultrafast laser radiation transfer in heterogeneous tissues using discrete ordinates method, Appl. Opt. 42 (16) (2003) 2897–2905.

[19] S.K. Wan, Z. Guo, S. Kumar, J. Aber, B.A. Garetz, Noninvasive detection of inhomogeneity in turbid media time-resolved log-slope analysis, J. Quant. Spectrosc. Radiat. Transfer 84 (4) (2004) 493–500.

[20] F. Liu, K.M. Yoo, R.R. Alfano, Ultrafast laser-pulse transmission and imaging through biological tissues, Appl. Opt. 32 (4) (1993) 554–558.

[21] M.Q. Brewster, Y. Yamada, Optical properties thick, turbid media from picosecond time resolved light scattering measurements, Int. J. Heat Mass Transfer 38 (1995) 2569–2581.

[22] G. Zaccanti, P. Bruscaglioni, A. Ismaelli, L. Carraresi, M. Gurioli, Q. Wei, Transmission of a pulse thin light beam through thick turbid media: experimental results, Appl. Opt. 31 (12) (1992) 2141–2147.

[23] Z. Guo, S. Kumar, K.C. San, Multidimensional Monte Carlo simulation of short-pulse laser transport in scattering media, J. Thermophys. Heat Transfer 14 (4) (2000) 504–511.

[24] Z. Guo, J. Aber, B. Garetz, S. Kumar, Monte Carlo simulation and experiments of pulsed radiative transfer, J. Quant. Spectrosc. Radiat. Transfer 73 (2002) 159–168.

[25] M.S. Patterson, B. Chance, B.C. Wilson, Time-resolved reflectance and transmittance for the noninvasive measurement of tissue optical properties, Appl. Opt. 28 (1989) 2331–2336.

Zhixiong Guo is an Assistant Professor of Mechanical and Aerospace Engineering and Biomedical Engineering Graduate Program at Rutgers University, New Brunswick/Piscataway. He received his B.S., M.S., and Doctor of Engineering in Engineering Physics from Tsinghua University, Beijing, in 1989, 1991, and 1995, respectively. Following several years as a researcher for KAIST in South Korea and for Tohoku University in Japan, he entered Polytechnic University in, Brooklyn New York, and received his Ph.D. degree in Mechanical Engineering in 2001. His current research interests are in laser applications in biology and medicine with foci on biomedical optical imaging, nano/bio-photonics, and heat transfer. He has published over 30 peer-reviewed publications in archival journals.

Siew Kan Wan graduated from Rutgers University in 2002. He is now a graduate student under the direction of Professor Guo and is expecting a M.S. degree in 2004.

David A. August graduated from the Massachusetts Institute of Technology in 1976 and received his M.D. degree form Yale Medical School in 1980. Following his general surgery training at Yale and a Surgical Oncology Fellowship at the National Cancer Institute, he has developed an academic career in Surgical Oncology. He is currently an Associate Professor of Surgery and the Chief of the Division of Surgical Oncology at UMDNJ/Robert Wood Johnson Medical School and The Cancer Institute of New Jersey. His current research interests include medical imaging to screen for and detect cancer, and food based approaches to cancer chemoprevention.

Jinpin Ying obtained a Ph.D. degree in Biomedical Optics from Zhejiang University in China in 1996. He is a Senior Member of Technical Staff at Bell Labs, Lucent Technologies.

Stanley M. Dunn is an Associate Dean for Industrial Outreach at School of Engineering, and Paul S. and Mary W. Monroe, Faculty Scholar at Rutgers University. He was the Editor-in-Chief (1996–2001) for Journal of Computer Assisted Microscopy. He is an associate Editor for Pattern Recognition and for International Journal of Imaging Science and Technology.

John L. Semmlow received the BSEE degree from the University of Illinois in Champaign in 1964 and the Ph.D. degree in Bioengineering from the University of Illinois Medical Center in Chicago in 1970. He has held faculty positions at the University of California, Berkeley, and the University of Illinois, Chicago, and currently holds a joint position as Professor of Surgery, UMDNJ-Robert Wood Johnson Medical School and Professor of Biomedical Engineering at Rutgers University, New Jersey. He was appointed a Fellow of the IEEE in 1994 in recognition of his work in acoustic detection of coronary artery disease. He is founding chair of the International Conference on Vision and movement in Man and Machines last held in 2002 in Marseille, France. His active research areas include physiological motor control and medical instrumentation with an emphasis on noninvasive instrumentation.